Solar radiation (PAR, UV-A, UV-B) penetration in a shallow maturation pond operating in a tropical climate

Daniel F. C. Dias and Marcos von Sperling

ABSTRACT

Solar radiation is considered the primary route for disinfection of pathogenic bacteria in maturation ponds. There is scarce information on depth profiling and attenuation of photosynthetically active radiation (PAR), UV-A and UV-B in shallow maturation ponds operating in tropical climates. Measurements of solar irradiance of the three wavelength ranges, together with turbidity, have been acquired from different depths for over 1 year in a shallow maturation pond (44 cm of depth) operating in Brazil. UV-A and UV-B were still detected at 10 cm from the surface, but from 15 cm both were undetectable. PAR was still detected at 30 cm of depth. Irradiation attenuation showed to be related to turbidity. Attenuation coefficients were calculated and simple models without turbidity (traditional structure) or including $\log_{10}$ of turbidity are proposed for predicting PAR irradiance attenuation as a function of depth.

Key words | light attenuation coefficient, shallow maturation pond, solar irradiance, wastewater treatment

Daniel F. C. Dias (corresponding author)
Marcos von Sperling
Department of Sanitary and Environmental Engineering,
Federal University of Minas Gerais,
Av. Antônio Carlos 6627 – Escola de Engenharia, Bloco 1 – sala 4622,
Belo Horizonte 31270–901,
Brazil
E-mail: *danielfcdias@hotmail.co.uk*

INTRODUCTION

Sunlight is an abundant, free and natural resource and considered a major disinfection factor in waste stabilisation ponds (WSPs). It has long been recognised to have a lethal effect on enteric bacteria in water bodies (Fujioka *et al.* 1981), where the bacterial die-off rate is considered proportional to sunlight intensity (Moeller & Calkins 1980; Polprasert *et al.* 1983; Whitlam & Codd 1986; Gersberg *et al.* 1987; Curtis *et al.* 1992a, 1994).

Photosynthetically active radiation (PAR) and ultraviolet (UV) are of particular interest in WSPs for pathogen inactivation (Hartley & Weiss 1970; Curtis *et al.* 1992a, 1992b; Curtis *et al.* 1994; Davies-Colley *et al.* 1999, 2000; Muela *et al.* 2002; Sinton *et al.* 2002; Holzinger & Lütz 2006; Whitman *et al.* 2008; Maïga *et al.* 2009; Bolton *et al.* 2010, 2011; Silverman *et al.* 2013). Sunlight is an effective agent in wastewater disinfection concerning bacteria and viruses, and has the advantage of not producing or contributing to the formation of toxic by-products (Metcalf and Eddy, Inc. 2013). Disinfection can also be done with special UV lamps that reproduce UV-C, the strongest wave for disinfection, but maintenance costs are higher compared with natural sunlight disinfection in ponds (energy requirements and lamp replacement). In developing countries from Latin America, disinfection through WSPs is the most widely used treatment system (Noyola *et al.* 2012). UV radiation intensity received by ponds is not controllable when compared with systems using UV lamps for disinfection, and consequently efficiency can vary with shading, turbidity, latitude, altitude, and time of day and year (WHO 2002). A simple characterisation for PAR and UV is as follows.

- Visible light radiation or PAR (400–700 nm) is what the human eye can see and detect. Every type of light that can be seen is considered visible light, whether it is emitted by stars or light bulbs.
- UV radiation has as its natural source the sun. Generally known to the public due to its ability to tan and cause sun burns, it also produces harmful effects on bacteria if exposed. Its wavelengths are ultraviolet A (UV-A: 320–400 nm) and ultraviolet B (UV-B: 290–320 nm).

UV-B is the strongest natural disinfectant for bacteria, but only accounts for about 0.2% of total solar irradiance

doi: 10.2166/wst.2017.203

reaching the surface at noon. UV-A totals about 5% and visible light represents around 50% of the total solar irradiance at noon (Shilton 2005). These percentages were used in calculations undertaken in this study in order to estimate UV-B, UV-A and PAR irradiance reaching the pond's surface.

In natural water bodies, Haag & Hoigne (1986) concluded that virtually all effective light was attenuated fully up to 1.0 m in depth. Balogh *et al.* (2009) confirmed that UV-B radiation was limited to the first few centimetres in turbid water bodies, but in clear and deep water bodies it can penetrate several metres; thus UV-B being dependent on not only attenuation rates, but also depth and mixing processes (De Lange 2000). Bolton *et al.* (2011) characterised the extinction rate of sunlight in a facultative pond (1.5 m) by measuring PAR, UV-A and UV-B with submersed sensors. UV-B and UV-A penetrations were limited to 8 cm and 15 cm in depth, respectively, and PAR penetrated further (43 cm). Kohn & Nelson (2007) considered that 99% of UV-B and PAR is absorbed in the first 2.5 cm and 8 cm, respectively. Sunlight attenuation (through absorption and scattering) is very strong in maturation ponds due to high turbidity associated with large algal concentrations, producing different light attenuation properties in different ponds (Curtis *et al.* 1994), and this is even more pronounced for the UV spectrum.

There is scarce information on depth profiling and attenuation of PAR, UV-A and UV-B in shallow maturation ponds operating in tropical climates. The reason for performing depth profiling and calculating attenuation coefficients for pond systems operating in tropical climates is that these are the most applied type of technology in Latin America, as pointed out by Noyola *et al.* (2012). This is because in tropical climates, the sun's angle is higher than in temperate climates, and because seasonally there is little difference between the warmer months and cooler months, as shown by Dias *et al.* (2014) when comparing two different seasons of a similar treatment line operating in the same location. This results in maturation ponds operating with very good removal efficiencies in terms of solar-mediated disinfection. The objective of this research was to collect data of solar irradiance from the surface and different depths of a shallow maturation pond (44 cm) over 1 year of continuous monitoring. A physicochemical parameter associated with attenuation rates (turbidity) was also intensively sampled over the research period.

METHODS

Experimental apparatus

The treatment line is composed of the following units in series treating urban wastewater: an upflow anaerobic sludge blanket reactor followed by two maturation ponds (the first pond without baffles and the second pond with longitudinal baffles) and a graded rock filter, designed to serve a population of 250 inhabitants (40 $m^3 \cdot d^{-1}$). The treatment line is located in Belo Horizonte, Brazil, latitude 19°53′ S, longitude 43°52′ W, altitude 852 m, in Cfa or Cwa humid subtropical climate according to the Köppen classification. The focus of this research was on the second pond of the series with a shallow depth of 44 cm. The accumulated sludge in the pond was previously removed before the research. The longitudinal baffles inside the pond do not influence or interfere with sunlight penetration, and their importance is on pathogenic organism removal, which is not directly covered here.

Solar intensity/irradiance reaching the pond surface and different depths in the liquid column

Two different sets of sensors were used. An onsite weather station, the Wireless Vantage Pro 2® by Davis Instruments® (Figure 1(a)), acquired the total solar irradiance reaching the surface and atmospheric pressure. Total solar irradiance, expressed in $W \cdot m^{-2}$, was stored every 10 min on a data logger. Atmospheric pressure was also recorded and used the same sampling interval. The wavelength range covered by the weather station is from 300 nm to 1,100 nm (includes most of the UV spectrum and the whole of PAR). The meteorological station was installed in accordance with the Brazilian legislation for weather monitoring and recommendations made by Davis Instruments.

A set of UV-A (SKU 421/I 43814), UV-B (SKU 430/I 43815) and PAR (SKL 2623/I 43817) sensors was placed at different depths (5, 10, 15, 20 and 30 cm) in the water column of the pond and recorded the amount of irradiance (Figure 1(b)) on a data logger (datahog 2®). The set of sensors, data logger and levelling plate were acquired from Skye Instruments®. The PAR sensor recorded irradiance between 400 and 700 nm, and ultraviolet A (UV-A) and ultraviolet B (UV-B) sensors recorded irradiance between 315 and 400 nm and between 280 and 315 nm, respectively.

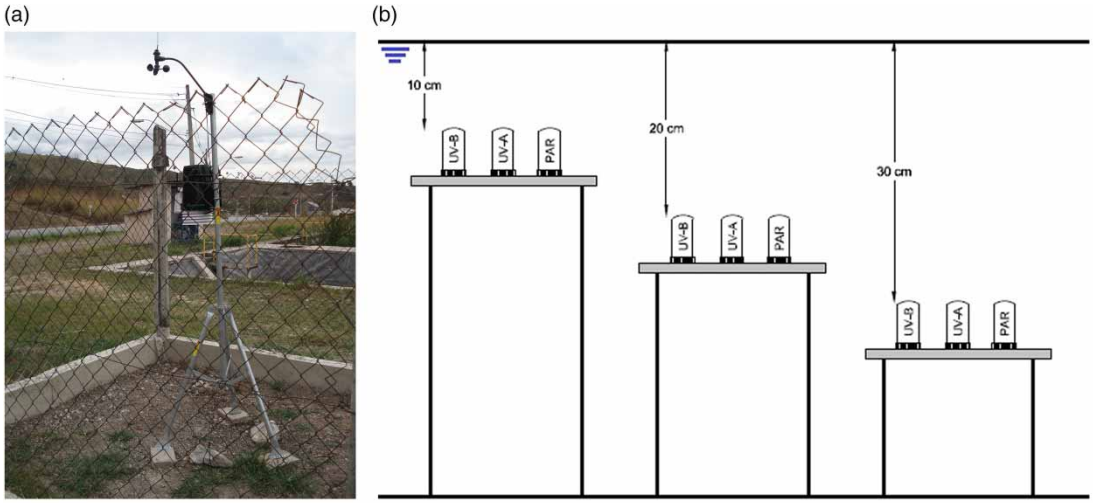

Figure 1 | (a) Meteorological weather station for monitoring total solar irradiance and atmospheric pressure; (b) example of UV-A, UV-B and PAR sensor placement inside the pond.

The sensors were placed at different levels each week for continuous readings and measuring of UV-A, UV-B and PAR, as shown in Table 1 and Figure 1(b)).

Over a period of 1 year, turbidity was measured every hour on given days of the week of every month, in order to assist in the characterisation of the optical conditions in the pond.

Surface UV-A, UV-B and PAR irradiances were estimated by multiplying total solar irradiance by the percentages proposed by Shilton (2005) for irradiances at noon, for a time interval from 9:00 to 16:00. Another form of predicting UV-A, UV-B and PAR was by applying a program used by Silverman *et al.* (2015), a Simple Model of the Atmospheric Radiative Transfer of Sunshine (SMARTS – global horizontal irradiance). The program was developed and tested by Gueymard (1995, 2001) and estimates the amount of surface UV-A, UV-B and PAR irradiance based mainly on geographic positioning and atmospheric pressure. SMARTS considers 24-hour and seasonal changes in light intensity, but clear-sky conditions are assumed and it does not account for differences in atmospheric conditions.

Solar irradiance attenuation

Light can be measured as irradiance (I), which represents the number of photons per unit area of time ($m^{-2}{\cdot}s^{-1}$) or by the amount of energy per unit of time ($W{\cdot}m^{-2}$). $Id_{(z)}$, downward irradiance intensity at a given depth, attenuates with depth and can be described by Equation (1), following Beer–Lambert's law (Curtis *et al.* 1994). Attenuation coefficients (K_a) were calculated using Equation (1). K_a considers both absorption and scattering of light, and therefore can be described as a function of the light attenuation

Table 1 | Example of measuring programme for UV-A, UV-B, PAR and turbidity at different depths

Month	Measurement days	Time of monitoring per day (hours)	Sampling interval (minutes)	Depth profiling – from water surface of pond (cm)	Parameters measured in the field
1st month	1st week	24	10	5–10[a]	UV-A, UV-B and PAR; turbidity
	2nd week			15–20[a]	
	3rd week			30	
	4th week			5–10[a]	
2nd month	1st week			15–20[a]	
	2nd week			30	
	3rd week			5–10[a]	
	4th week			15–20[a]	

[a]Depth placement changes every time for different weeks in order to obtain more points throughout the depth and produce a better profile.

properties within the pond environment.

$$Id_{(z)} = Id_{(0)}.e^{-K_a.Z} \quad (1)$$

where

- $Id_{(z)}$ – downward irradiance at a depth z ($m^{-2}\cdot s^{-1}$) or ($W\cdot m^{-2}$);
- $Id_{(0)}$ – downward irradiance at the surface ($m^{-2}\cdot s^{-1}$) or ($W\cdot m^{-2}$);
- $K_{a(z)}$ – attenuation coefficient for downward irradiance (m^{-1});
- Z – depth from surface or reference point (m).

Mean attenuation coefficients (K_a) for PAR, UV-A and UV-B were calculated based on the pairs of irradiance and depth, for which $Id_{(z)}$ were the mean irradiance values and Z the depths at which irradiance was measured. For the surface of the pond (Z = 0 m), irradiance for UV-A, UV-B and PAR was estimated based on the ratios recommended by Shilton (2005), presented in the 'Introduction', multiplied by the total solar irradiance arriving at the surface ($Id_{(0)}$). The other method used the SMARTS program to estimate surface UV-A, UV-B and PAR. Several pairs of PAR I-Z (irradiance-depth), i.e., 0, 10, 20 and 30 cm, were used to estimate K_a through non-linear least squares method, and applying the Solver tool in Excel for finding the value of K_a that minimised the sum of the squared errors.

As suggested by Bolton *et al.* (2011), turbidity was also measured during the whole experiment every hour for 4 hours on selected days, either in the morning or afternoon by using a column sampler to sample up to the depth of the irradiance sensors.

RESULTS AND DISCUSSION

Overall total solar irradiance reaching the pond's surface is presented in Figure 2 for the whole monitoring period (12 July 2014 to 30 November 2015) and condensed into 1 day, representing over 1 year and 4 months of continuous monitoring. Time is divided up in 10 minute intervals. The variability of total solar irradiance increased closer to noon and then proceeded to decrease, therefore highlighting the influence of different seasons and cloud cover on the amount of irradiance reaching the surface when the sun is at its highest point in the sky. The highest mean value was 688 $W\cdot m^{-2}$ at 12:50:00. Overall, solar irradiance was detected from 05:30:00 until 19:40:00.

Irradiance depth profiling of the five depths started in June 2014 and continued until November 2015 (1 year and 5 months) of continuous sampling (Table 1). As expected, the amount of solar irradiance recorded at different depths in the pond diminished as depth increased (Figure 3). UV-A and UV-B were only detected at 5 cm and 10 cm in depth, and from 15 cm onwards only PAR persisted due to its longer wavelength characteristics. The plotted data (mean values) in Figure 3 are for the whole monitoring period, representing all four seasons, and condensed into 1 day.

At 5 cm in depth, Figure 3(a), UV-A virtually mimics PAR and both followed a steep slope until their maximum mean value at 12:10:00, then proceeded to decrease sharply

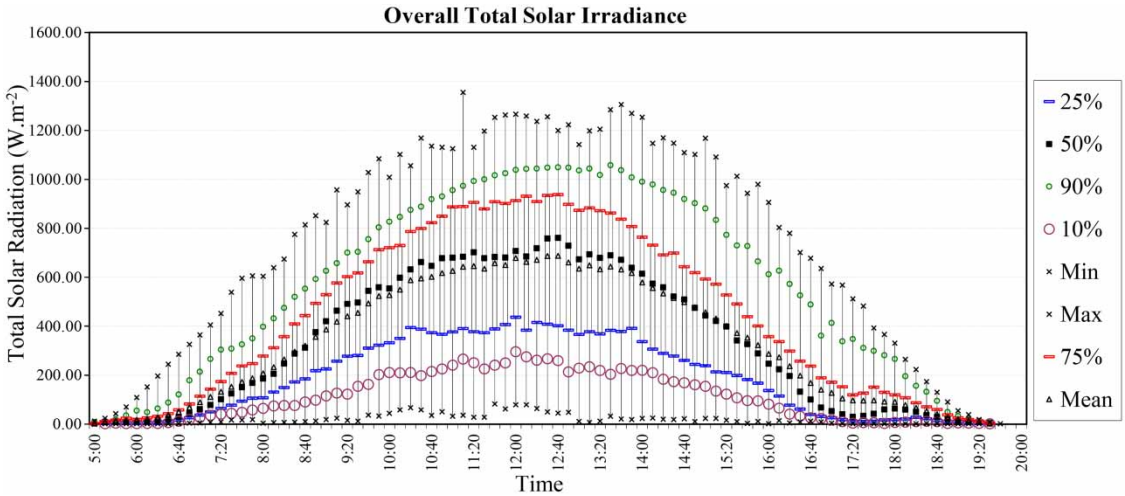

Figure 2 | Hourly profile of total solar irradiance reaching the surface of the ponds over the monitoring period.

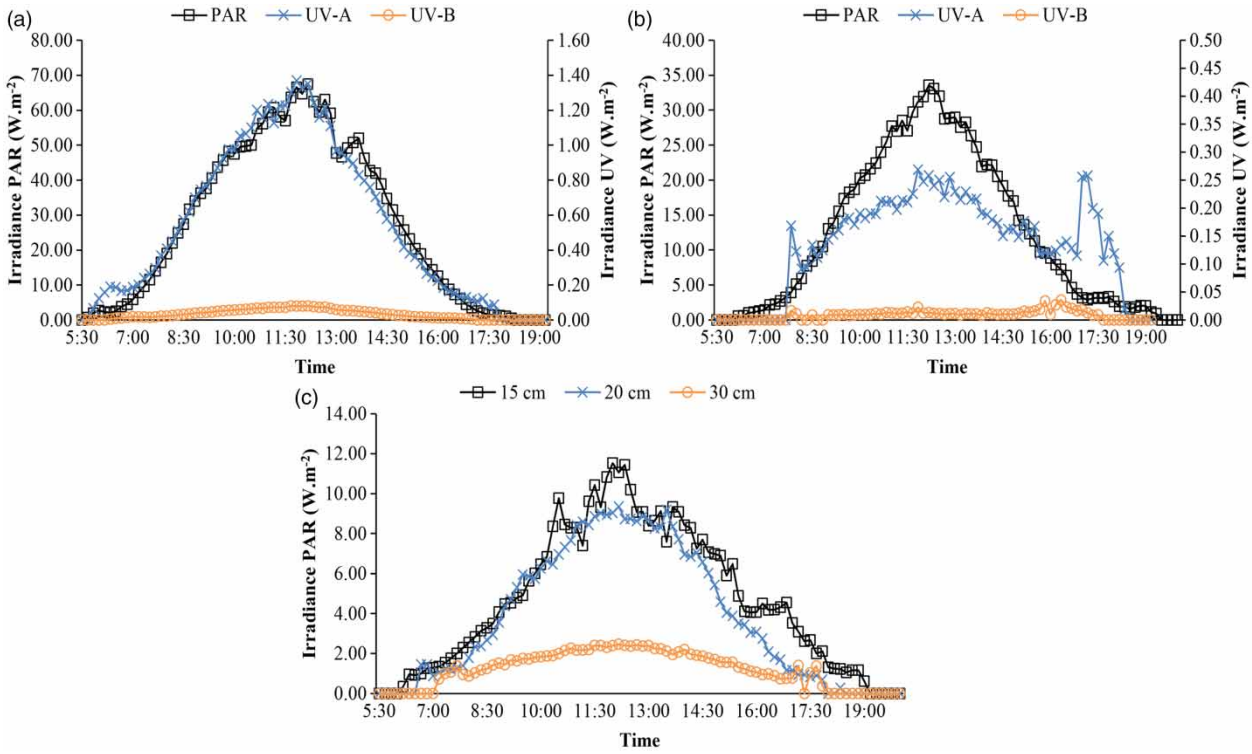

Figure 3 | (a) UV-A, UV-B and PAR irradiance reaching 5 cm in depth in the shallow pond; (b) UV-A, UV-B and PAR irradiance reaching 10 cm in depth in the shallow pond; (c) PAR irradiance reaching 15, 20 and 30 cm in the pond. Note that the Y-axis scales are different.

until completely attenuating at the end of the day. UV-B on the contrary produced a gentle slope until 12:10:00 and then proceeded to decrease until completely attenuating. Although the wavelengths are different in nature, they all behaved the same way and increased and decreased at the same time. As expected, the plotted data of each wavelength followed a bell-like shape, the same as total solar irradiance (Figure 2).

At 10 cm in depth, the bell-like shape was present for PAR (Figure 3(b)) and not affected by pond optics. UV-A and UV-B presented a distorted and irregular shape that can be attributed to pond optics – Figure 3(b) shows that both waves are very much attenuated and affected by them. UV-A presented two peak values at around 11:50:00 and 16:50:00 and UV-B followed this tendency as well (Figure 3(b)).

The UV spectrum was undetectable at 15 cm depth and only PAR was recorded and presented in Figure 3(c). The bell-like shape was still present at 15, 20 and 30 cm (Figure 3(c)), but slightly more distorted. Note that each wavelength was detected before the other at different depths, whereas 15 cm was recorded earlier and extinguished later when compared with the other two depths (20 cm and 30 cm). PAR at 30 cm presented a more flattened shape and therefore was less energised when compared to the other depths (15 cm and 20 cm), but still retained its bell-like shape. This can be attributed to the pond optics, where the distribution of PAR at 30 cm was dispersed and smoothed by light scattering and attenuating particles.

Figure 4 shows how K_a values for UV-A, UV-B and PAR, regarding turbidity, behaved over time. A comparison between the three K_a values is also shown. Surface irradiance was estimated using the percentages recommended by Shilton (2005) and the SMARTS program, but the K_a values shown in Figure 4 are relative to surface irradiance calculated by the percentages as given by Shilton (2005). The K_a values estimated based on the SMARTS program were only used for modelling PAR attenuation. The time period used was between 9:00 and 16:00 because multiple turbidity sampling was performed during this time period.

Turbidity values in all three graphs are the same (Figure 4). Turbidity seemed to increase from 09:00 until 10:00, decreased between 10:00 and 11:00, and then finally increased from 11:00 to 13:00, reaching a peak value of 89 NTU at 10:00 and 13:00. From 13:00 it decreased to its lowest value at 16:00. Turbidity was condensed from all

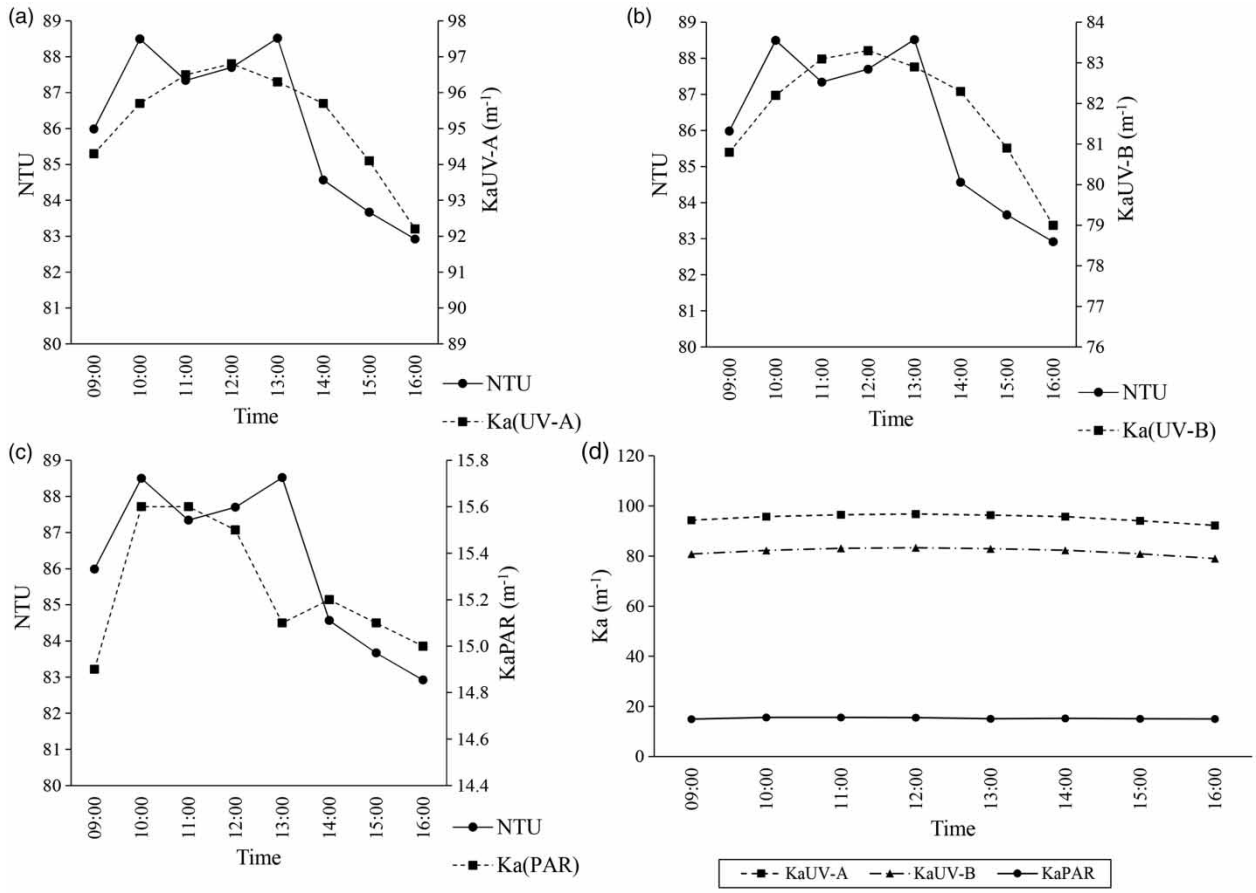

Figure 4 | (a) Turbidity versus K_aUV-A over time; (b) turbidity versus K_aUV-B over time; (c) turbidity versus K_aPAR over time; (d) attenuation rates of UV-A, UV-B and PAR.

depths into one mean turbidity value for each different hour and this can explain the erratic tendencies over the day. Attenuation rates (K_a) of UV-A and UV-B increased from morning until reaching the highest value at 12:00 and then proceeded to decrease (Figure 4(a) and 4(b)), following a very similar trend to turbidity. K_aPAR increased and peaked at 10:00 (same time as turbidity peaked) and then started to decrease. An increase in attenuation only occurred again at 14:00 after a high peak in turbidity at 13:00. This suggested that, as expected, turbidity affected the attenuation rate of PAR. Note that in Figure 4(d), UV-A attenuated faster than UV-B, which was not expected. This tendency was also observed when considering the estimated surface irradiances with the SMARTS program used to calculate K_a. UV-A could be attenuating more than UV-B in this experiment because of more efficient scattering and/or absorption properties in the medium of the photons in the 315 to 400 nm range.

Due to the vast amount of data collected for PAR at each depth, Equation (1), with its traditional structure was used (reproduced in Equation (2)), with the calculated value of K_a. K_a for PAR was calculated using the Solver tool in Excel, minimising the sum of the squared errors. Two other equations were investigated (Equations (3) and (4)), on the basis that turbidity (TUR) and the $\log_{10}$ of turbidity (LOG_{10}(TUR)) influenced the attenuation coefficient. All equations are for a timeline of 09:00–16:00. Table 2 shows the estimated K_a values for the three equations, considering the two different methods for assessing surface PAR (fixed percentages by Shilton (2005) or SMARTS program), as well as the resulting coefficient of determination (CoD) of the three models. Figure 5(a)–5(c) show the goodness-of-fit in terms of the plot of observed results vs calculated results for Shilton's (2005) method for determining surface PAR based on fixed percentages, due to its higher simplicity.

$$Id_{(z)} = Id_{(0)}.e^{-K_a.Z} \quad (2)$$

$$Id_{(z)} = Id_{(0)}.e^{-K'_a.TUR.Z} \quad (3)$$

Table 2 | K_a values, coefficient of determination and K_a units for Equations (3)–(5)

Method used to estimate surface PAR	Equation	K_a	Coefficient of determination	K_a unit
Shilton (2005)	2	24.7	0.85	K_a (m^{-1})
	3	0.28	0.72	K_a' (m^{-1}·NTU^{-1})
	4	12.7	0.83	K_a'' (m^{-1}·$LOG_{10}(NTU^{-1})$)
SMARTS	2	27.7	0.80	K_a (m^{-1})
	3	0.31	0.74	K_a' (m^{-1}·NTU^{-1})
	4	14.1	0.79	K_a'' (m^{-1}·$LOG_{10}(NTU^{-1})$)

Coefficient of determination values can vary between $-\infty$ and $+1$. Values close to $+1$ indicate good fitting.

$$Id_{(z)} = Id_{(0)}.e^{-K_a''.LOG_{10}(TUR).Z} \quad (4)$$

where

- $Id_{(z)}$ irradiance at depth z (m^{-2}·s^{-1}) or (W·m^{-2});
- $Id_{(0)}$ irradiance at the pond surface (m^{-2}·s^{-1}) or (W·m^{-2});
- K_a – attenuation coefficient for downward irradiance (m^{-1});
- K_a' – attenuation coefficient for downward irradiance considering turbidity (m^{-1}·NTU^{-1});
- K_a'' – attenuation coefficient for downward irradiance considering log10(turbidity) (m^{-1}·$LOG_{10}(NTU^{-1})$);
- TUR – turbidity (NTU);
- Z – depth from surface or reference point (m).

Equations (2) and (4) produced the best fit when analysing observed irradiance versus estimated irradiance (Figure 5(a)) for Shilton (2005) percentages used to determine surface PAR, presenting a CoD of 0.85 and 0.83, respectively (Table 2) and indicating a good fit. This suggested that LOG_{10}(TUR) could be included in the model for PAR attenuation, but probably a better fit could have been observed if the range of measured turbidity had

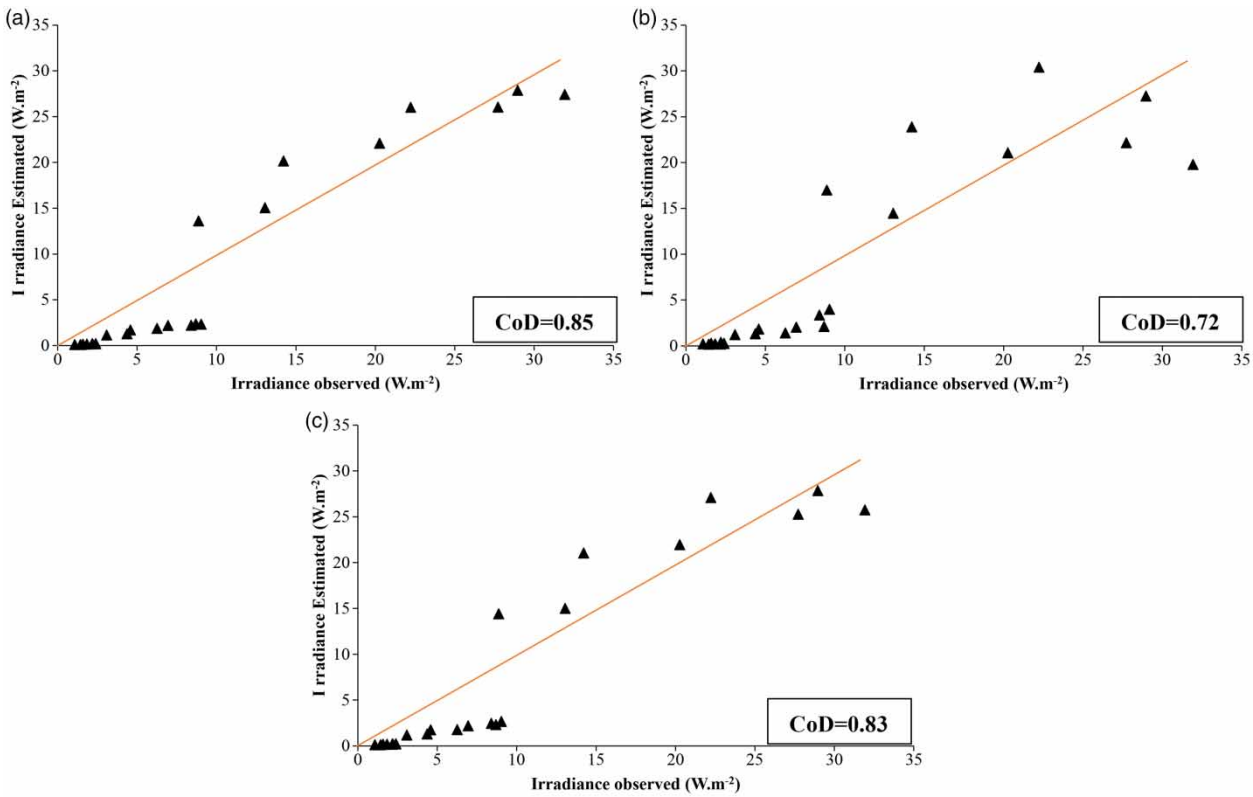

Figure 5 | (a) Observed and estimated irradiance for Equation (2); (b) observed and estimated irradiance for Equation (3); (c) observed and estimated irradiance for Equation (4). All results consider surface irradiance based on Shilton (2005) percentages. All graphs show the 45° line of theoretical perfect fitting.

been larger. Figure 5(b) corresponds to the plotted observed and estimated irradiance from Equation (3), and using just turbidity did produce as good a fit as Equations (2) and (4). By applying the logarithm of turbidity (Figure 5(c)), as done by Bolton *et al.* (2011), the observed and estimated values followed a more linear trend, approaching that of Figure 5(a) and resulting in a better CoD. In fact, as suggested by Bolton *et al.* (2011), turbidity could indeed be a good indicator of attenuation (as indicated by the high CoD) and also a simple parameter to measure in any pond system, but this was not as evident in this study because of the low variability of the measured turbidity values. On the other hand, observing Figure 4(a)–4(c) it can be seen that turbidity mimics the tendency of the attenuation rate for each hour, or vice versa, by increasing to a maximum and then decreasing, especially for UV-A and UV-B with peak values of irradiance and turbidity occurring at roughly the same time. Considering the SMARTS program for estimating surface PAR, CoD values were slightly inferior to the other method (except for Equation (3)), therefore also indicating good fits and also suggesting LOG_{10}(TUR) could be included in the model. Note that in Table 2 the attenuation coefficients are presented in different units and cannot be compared directly with each other.

Table 3 shows the minimum and maximum measured values of turbidity (09:00 to 16:00) and total solar surface irradiance (TSI – midday) and the resulting UV-A, UV-B and PAR irradiance from the different depths (midday) during the monitoring period. The minimum and maximum values of TSI and turbidity can give boundary conditions for the calculation of the attenuation coefficients from Table 2 and Equations (2)–(4), for shallow maturation ponds operating in similar tropical climatic conditions.

When planning to apply these equations for other pond systems, it should be noted that the pond studied here is shallow and turbidity did not change substantially along the depth on average, but the minimum and maximum turbidity values were quite far apart. Both methods, SMART program and fixed percentages as proposed by Shilton (2005), can be used for estimating surface UV-A, UV-B and PAR because they present very similar results. Although Shilton's (2005) percentages are a simple form of estimating the amount of UV-A, UV-B and PAR on the surface of the location, we do recommend that care should be taken when using these percentages for other locations because solar intensity varies due to latitude and altitude. Percentages of UV-A, UV-B and PAR should be estimated for each different location, as shown in Table 4, considering the SMARTS program estimation of UV-A, UV-B and PAR for the experimental period divided by the measured TSI during the same period. Therefore, in this particular case, it is possible to conclude that Shilton's (2005) percentages provided a sufficiently accurate estimation of surface UV-A, UV-B and PAR for this particular location of the pond.

Table 3 | Minimum and maximum values of turbidity, total surface solar irradiance, and irradiance (UV-A, UV-B and PAR) measured at depths of 5, 10, 15, 20 and 30 cm in the maturation pond

Variable	Minimum	Maximum
Turbidity (NTU)	22.8	201
TSI – 12:00 ($W \cdot m^{-2}$)	88	1,048
5 cm – 12:00 ($W \cdot m^{-2}$)		
UV-A	0.03	5.84
UV-B	0.01	0.34
PAR	4.12	220.37
10 cm – 12:00 ($W \cdot m^{-2}$)		
UV-A	0.02	1.00
UV-B	0.003	0.023
PAR	3.30	103.25
15 cm, 20 cm and 30 cm – 12:00 ($W \cdot m^{-2}$)		
PAR – 15 cm	1.99	50.73
PAR – 20 cm	0.55	22.17
PAR – 30 cm	0.27	7.69

TSI: total solar irradiance.

Regarding TSI in other locations in the globe, average regional data provided by NASA (2008), for three different latitudes representing tropical and equatorial conditions (20° S, 0°, 20° N), three longitudes (60° W, 0°, 60° E) and three periods (January, July, annual averages) are presented in Table 5. Average solar irradiance during January 2015

Table 4 | Percentage ratio between UV-A, UV-B and PAR irradiance estimated by SMARTS and total solar irradiance measured from the meteorological station

Time/Wave	UV-A/TSI	UV-B/TSI	PAR/TSI
09:00:00	11%	0.29%	86%
10:00:00	8%	0.26%	63%
11:00:00	8%	0.26%	60%
12:00:00	7%	0.24%	55%
13:00:00	7%	0.22%	52%
14:00:00	6%	0.18%	48%
15:00:00	6%	0.10%	48%
16:00:00	4%	0.02%	40%
Overall mean/*median*	7%/*7%*	0.20%/*0.23%*	57%/*54%*
Ratios proposed by Shilton (2005) for midday	5%	0.20%	50%

Table 5 | Average regional values of total surface solar irradiance ($W \cdot m^{-2}$) for different latitudes, longitudes and periods of the year

Latitude	Longitude	January	July	Annual
20° S	60° W	458	360	411
	0°	646	345	477
	60° E	642	336	496
0°	60° W	410	389	408
	0°	452	452	466
	60° E	506	423	505
20° N	60° W	432	551	504
	0°	389	654	529
	60° E	388	603	526
19°53 S (measured at experimental site)	43°52′ W	485	347	396

Source: adapted from NASA (2008).

and July 2015, and annual solar irradiance (between December 2014 and November 2015) at the experimental plant are also shown.

These values are given here in order to show the influence of the geographical location and time of the year, but can be used in order to have a first estimate of regional surface solar irradiance for these different locations. For other regions in the globe, the NASA (2008) reference can be used. The original NASA data are presented as $kWh \cdot m^{-2} \cdot d^{-1}$, and have been converted here to $W \cdot m^{-2}$ by multiplying by $(1{,}000\ W \cdot kW^{-1}) \times (1\ d.\ Y\ h^{-1})$. The Y value represents the number of sunlight hours per day for each geographical location, calculated as the difference between sunrise and sunset hours. These have been obtained for the relevant latitudes and longitudes based on the 15th day of each month during 2015, from NOAA (2016). Higher irradiances in January can be found in the southern hemisphere, whereas higher irradiances occur in July in the northern hemisphere, both reflecting summer conditions.

CONCLUSIONS

The following conclusions can be made after PAR, UV-A and UV-B irradiance at the surface of the pond were estimated using fixed percentages related to measured values of the total solar irradiance and also a specific model (SMARTS program), and PAR, UV-A and UV-B irradiance measured at various depths inside a shallow maturation pond over an extensive period of time.

- Results from total solar irradiance indicated cloud cover, seasons and atmospheric conditions affected irradiance levels greatly. Consequently, this affected the amount of solar irradiance recorded at different depths in the shallow maturation pond (height of 44 cm).
- Solar irradiance depth profiling showed that UV-A and UV-B penetrated in the pond up to 10 cm and were not detected at 15 cm depth, therefore potentially impacting overall disinfection in the pond. Moreover, these two wavelengths were very much affected by pond optics when compared to the stronger PAR wave, and produced a very irregular shape at 10 cm depth.
- PAR penetrated the pond up to at least 30 cm.
- Turbidity seems to follow the same tendency as the attenuation coefficient for UV-A and UV-B, or vice versa. The attenuation coefficient was calculated using three different models (without turbidity, with turbidity, and with $\log_{10}$ of turbidity). Even though the fitting of the models without turbidity and with $\log_{10}$ of turbidity was good for both models considered for estimating surface PAR, care should be taken in applying them to other ponds, due to the specificities associated with the pond under study (shallow depth and no expressive variation of the turbidity with depth).

ACKNOWLEDGEMENTS

The authors would like to thank COPASA and the Brazilian agencies CAPES, CNPq and FAPEMIG for their support to the research. Also this research was part of an international program financed by the Bill & Melinda Gates Foundation for the project 'Stimulating local innovation on sanitation for the urban poor in Sub-Saharan Africa and South-East Asia' under the coordination of UNESCO-IHE, Institute for Water Education, Delft, The Netherlands. Thanks are also extended to Dr Kara L. Nelson from the University of California, Berkeley, who provided the SMARTS program, and Dr Matt Verbyla for providing the NASA data.

REFERENCES

Balogh, K., Németh, B. & Vörös, L. 2009 Specific attenuation coefficients of optically active substances and their contribution to the underwater ultraviolet and visible light climate in shallow lakes and ponds. *Hydrobiologia* **632** (1), 91–105.

Bolton, N. F., Cromar, N. J., Hallsworth, P. & Fallowfield, H. J. 2010 A review of the factors affecting sunlight inactivation of micro-organisms in waste stabilisation ponds: preliminary results for enterococci. *Water Science and Technology* **61** (4), 885–890.

Bolton, N. F., Cromar, N. J., Buchanan, N. A. & Fallowfield, H. J. 2011 Variations in sunlight attenuation in waste stabilisation ponds and environmental waters. In: *9th IWA Specialist*

Conference on Waste Stabilisation Ponds Adelaide, South Australia, Australia.

Curtis, T. P., Mara, D. D. & Silva, S. A. 1992a Influence of pH, oxygen, and humic substances on ability of sunlight to damage faecal coliforms in waste stabilization pond water. *Applied and Environmental Microbiology* **58**, 1335–1343.

Curtis, T. P., Mara, D. D. & Silva, S. A. 1992b The effect of sunlight on faecal coliforms in ponds: implications for research and design. *Water Science and Technology* **26** (7–8), 1729–1738.

Curtis, T. P., Mara, D. D., Dixo, N. G. H. & Silva, S. A. 1994 Light penetration in waste stabilization ponds. *Water Research* **28** (5), 1031–1038.

Davies-Colley, R. J., Speed, D. J., Ross, C. M. & Nagels, J. W. 1999 Inactivation of faecal indicator micro-organisms in waste stabilisation ponds: interactions of environmental factors with sunlight. *Water Research* **33** (5), 1220–1230.

Davies-Colley, R. J., Donnison, A. M. & Speed, D. J. 2000 Towards a mechanistic understanding of pond disinfection. *Water Science and Technology* **42** (10), 149–158.

De Lange, H. J. 2000 The attenuation of ultraviolet and visible radiation in Dutch inland waters. *Aquatic Ecology* **34**, 215–226.

Dias, D. F. C., Posmoser-Nascimento, T. E., Rodrigues, V. A. J. & Von Sperling, M. 2014 Overall performance evaluation of shallow maturation ponds in series treating UASB reactor effluent: ten years of intensive monitoring of a system in Brazil. *Ecological Engineering* **71**, 206–214.

Fujioka, R. S., Hashimoto, H. H., Siwak, E. B. & Young, R. H. F. 1981 Effect of sunlight on survival of indicator bacteria in seawater. *Applied Environmental Microbiology* **41**, 690–696.

Gersberg, R., Brenner, R., Lyon, S. & Elkins, B. 1987 Survival of bacteria and viruses in municipal wastewater applied to artificial wetlands. In: *Aquatic Plants for Wastewater Treatment Using Artificial Wetlands* (K. Reddy & W. Smith, eds). Magnolia Publishing, Orlando, FL, USA, pp. 237–245.

Gueymard, C. 1995 *SMARTS, A Simple Model of the Atmospheric Radiative Transfer of Sunshine: Algorithms and Performance Assessment*. Professional Paper FSEC-PF-270-95. Florida Solar Energy Center, Cocoa, FL, USA.

Gueymard, C. 2001 Parameterized transmittance model for direct beam and circumsolar spectral irradiance. *Solar Energy* **71** (5), 325–346.

Haag, W. R. & Hoigne, J. 1986 Singlet oxygen in surface waters. 3. Photochemical formation and steady-state concentrations in various types of waters. *Environmental Science and Technology* **17** (2), 65–71.

Hartley, W. R. & Weiss, C. M. 1970 Light intensity and the vertical distribution of algae in tertiary oxidation ponds. *Water Research* **4** (11), 751–763.

Holzinger, A. & Lütz, C. 2006 Algae and UV irradiation: effects on ultrastructure and related metabolic functions. *Micron* **37** (3), 190–207.

Kohn, T. & Nelson, K. L. 2007 Sunlight-mediated inactivation of MS2 coliphage via exogenous singlet oxygen produced by sensitizers in natural waters. *Environmental Science and Technology* **41** (1), 192–197.

Maïga, Y., Denyigba, K., Wethe, J. & Ouattara, A. S. 2009 Sunlight inactivation of *Escherichia coli* in waste stabilization microcosms in a Sahelian region (Ouagadougou, Burkina Faso). *Journal of Photochemistry & Photobiology* **94** (2), 113–119.

Metcalf and Eddy, Inc. 2013 *Wastewater Engineering, Treatment and Reuse*. 5th edn. Mc Graw-Hill, New York.

Moeller, J. R. & Calkins, J. 1980 Bactericidal agents in wastewater lagoons and lagoon design. *Journal Water Pollution Control Federation* **52**, 2442–2451.

Muela, A., García-Bringas, J. M., Seco, C., Arana, I. & Barcina, I. 2002 Participation of oxygen and role of exogenous and endogenous sensitizers in the photoinactivation of *Escherichia coli* by photosynthetically active radiation, UV-A and UV-B. *Microbial Ecology* **44** (4), 354–364.

NASA 2008 *NASA Surface Meteorology and Solar Energy (SSE)*. Release 6.0 Data Set (Jan 2008). Available from: http://eosweb.larc.nasa.gov/sse/.

NOAA 2016 *NOAA Solar Calculator*. National Oceanic and Atmospheric Administration, US Department of Commerce. Available from: http://www.esrl.noaa.gov/gmd/grad/solcalc/.

Noyola, A., Padilla-Rivera, A., Morgan-Sagastume, J. M., Guereca, L. P. & Hernandez-Padilla, F. 2012 Typology of municipal wastewater treatment technologies in Latin America. *Clean – Soil, Air, Water* **40** (9), 926–932.

Polprasert, C., Dissanayake, M. G. & Thanh, N. C. 1983 Bacterial die-off kinetics in waste stabilisation ponds. *Journal Water Pollution Control Federation* **55**, 285–296.

Shilton, A. (ed.) 2005 *Pond Treatment Technology*. IWA Publishing, London.

Silverman, A. I., Peterson, B. M., Boehm, A. B., McNeill, K. & Nelson, K. L. 2013 Sunlight inactivation of human viruses and bacteriophages in coastal waters containing natural photosensitizers. *Environmental Science and Technology* **47** (4), 1870–1878.

Silverman, A. I., Nguyen, M. T., Schilling, I. E., Wenk, J. & Nelson, K. L. 2015 Sunlight inactivation of viruses in open-water unit process treatment wetlands: modeling endogenous and exogenous inactivation rates. *Environmental Science and Technology* **49** (5), 2757–2766.

Sinton, L. W., Hall, C. H., Lynch, P. A. & Davies-Colley, R. J. 2002 Sunlight inactivation of fecal indicator bacteria and bacteriophages from waste stabilization pond effluent in fresh and saline waters. *Applied and Environmental Microbiology* **68** (3), 1122–1131.

Whitlam, G. C. & Codd, G. A. 1986 Damaging effects of light on microorganisms, spec. *Publ. Soc. Gen. Microbiol.* **17**, 129–169.

Whitman, R. L., Przybyla-Kelly, K., Shively, D. A., Nevers, M. B. & Byappanahalli, M. N. 2008 Sunlight, season, snowmelt, storm, and source affect *E. coli* populations in an artificially ponded stream. *The Science of the Total Environment* **390** (2–3), 448–455.

WHO 2002 *Global Solar UV Index – A Practical Guide*, WHO, Geneva.

First received 17 August 2016; accepted in revised form 24 March 2017. Available online 8 April 2017